IEEE Transactions on Nuclear Science, Vol. NS-28, No. 3, June 1981

NON-LINEAR OPTICS FOR THE FINAL FOCUS OF THE SINGLE-PASS-COLLIDER*

K. L. Brown and J. E. Spencer
Stanford Linear Accelerator Center
Stanford University, Stanford, California 94305

Introduction

Richter has proposed a single-pass-collider (SPC) for electrons and positrons of energy E ≥ 50 GeV colliding once per bunch with a repetition rate of 180 Hz having a luminosity equal to or greater than 10^{30} $cm^{-2}sec^{-1}$.[1,2] To achieve this, beam intensities of 5×10^{10} particles/bunch focused to spot sizes of less than ±2 μm are necessary.

The purpose of the final focus system (FFS) is to demagnify the beam envelope in the Collider arc lattice to a size suitable for beam collisions at the interaction region. The final spot size is determined by the beam emittance, the beta function β^* at the IR, the momentum spread in the beam, and the quality of the FFS optics. In particular, if the focusing system is not chromatically corrected, the momentum dispersion in the beam can lead to a substantial degradation in the quality of the final focus. The objective is to design a FFS for 50 GeV/c within ~100 meters having an IR spot size σ_{xy} of approximately 2 μm for a beam emittance of $\varepsilon = 3 \times 10^{-10}$ m-rad and a momentum spread of $\delta = \pm 0.5\%$. This requires a $\beta_{x,y}$ equal to or less than 1 cm. In this report we consider the problems encountered in the design of a final focus system that will reliably provide the desired beam size for collisions.

The design of single-pass systems usually follows from second order, linear differential equations using the equivalent dipole and quadrupole fields of the actual magnets to be used. This is adequate for "good" magnets (i.e., those with acceptably pure central fields) and for small enough beam sizes ($\bar{\sigma}_x, \bar{\sigma}_y \ll g$) where g is the magnet gap opening and $\bar{\sigma}$ is the average, transverse, rms beam size through the magnet. While a system can generally be built that validates such a model it is clearly not optimal. Furthermore, it is difficult to determine just how small the input emittance must be, how good the magnets should be or the related question of misalignment sensitivity. Even for the rather small invariant emittance proposed for the SPC ($\sigma_x\sigma_{x'}\gamma = 3 \times 10^{-5}$ m-rad), the strong focusing requirements indicate the possibility of higher order aberrations both before the interaction and afterwards when the emittance has been blown up by the beam-beam interaction and the beam is being transported to a dump or external area. As a result, it is desirable to develop a mathematical model for systems of dipoles, quadrupoles, sextupoles and higher multipoles that is valid to all orders and includes such effects as radiative energy loss. This then allows us to accurately predict the absolute focal position in space, the transverse and longitudinal beam profiles as well as energy spreading and damping effects.

Optics of the Final Focus System (FFS)

The objective of the FFS is to provide an IR spot size of $\sigma_{x,y} = \sqrt{\beta_{x,y}\varepsilon} \lesssim 2$ μm for a beam emittance of $\varepsilon = 3 \times 10^{-10}$ m-rad, an energy of $E_B > 50$ GeV and a maximum energy spread about the central orbit of $\delta_{max} = \pm 0.5\%$. An FFS that satisfies these requirements is shown in Fig. 1 and consists of four telescopic half-wave optical modules. The total length of the system is 114 m and consists of quads, bends and sextupole elements. Only quadrupoles would be necessary for sufficiently small energy spread. The first two telescopic modules match the beta function of the arc lattice to the desired IR β^*. The last two modules are used to correct the chromatic distortions at the IR.

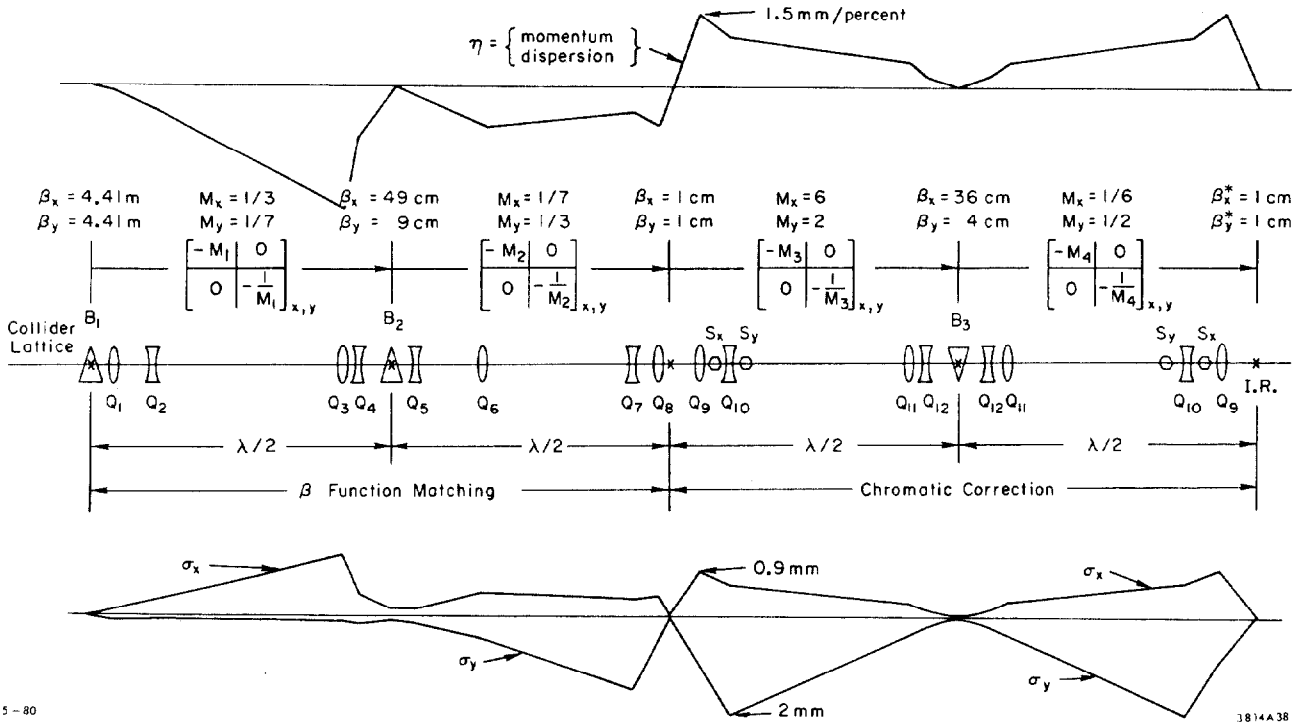

Fig. 1. Optical layout of the FFS showing the dispersion function (η_x) and betatron amplitudes ($\beta_{x,y}$).

* Work supported by the Department of Energy, contract DE-AC03-76SF00515.

0018-9499/81/0600-2568$00.75©1981 IEEE

Ray tracing the quadrupole array shown in Fig. 1 with the sextupoles turned off and using idealized, sharp-cutoff, pure quadrupole fields gave a monochromatic spot size of $\sigma_{x,y} = \sqrt{3}$ μm as predicted by linear theory. This increased to $\sigma_{x,y} = 2.0$ μm when realistic quads having the same effective field integrals but with fringe fields satisfying Maxwell's equations were used. Including an energy spread of $\delta_{max} = \pm 0.5\%$, as described in an appendix, increased these spreads to $\sigma_x = 5.7$ μm and $\sigma_y = 47$ μm. Thus, higher order geometric aberrations are acceptable but chromatic aberrations drastically increase the spot size and need to be corrected.

The chromatic broadening can be significantly reduced by placing sextupoles where the beam is momentum dispersed. Thus, a system of bends, quads and sextupoles is required with the bends providing the necessary dispersion and the sextupoles correcting the dominant second order chromatic aberrations in both transverse planes. It can be shown that the symmetry of the arrangement in Fig. 1 provides an optical system in which all second-order geometric and chromatic aberrations remain small. However, introduction of the dipole elements increases the energy spread and emittance via synchrotron radiation and the sextupoles introduce higher-order geometric and chromatic aberrations all of which must be minimized to achieve the smallest possible spot size at the IR. The most significant of these effects at 50 GeV was the higher-order optical aberrations. Figure 2 shows the fully corrected spot size at the IR for the configuration of Fig. 1 and the phase space description of Appendix 1. The rms standard deviations are:

$$\sigma_x^{IP} = \sigma_y^{IP} \leq 2.10 \text{ μm} \quad , \quad |\delta_{max}| \leq 0.5\% \quad .$$

Thus, the beam radius at the IR is essentially constant at 2 μm for all incident momentum spreads $\delta_{max} \lesssim \pm 0.5\%$.

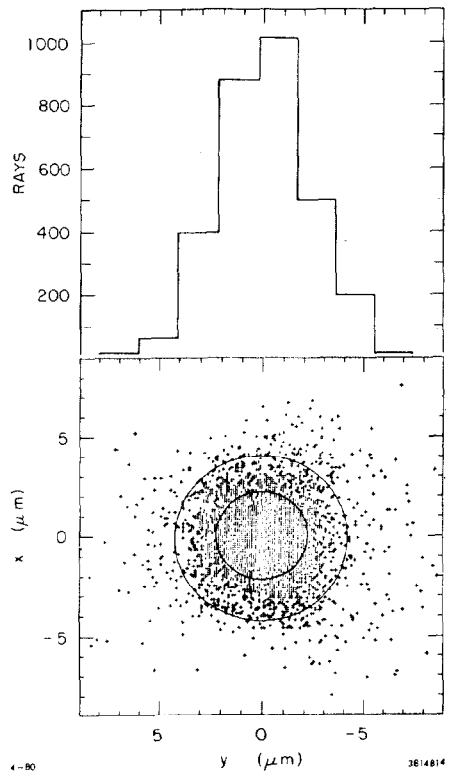

Fig. 2. Scatter plot of 3000 randomly selected rays traced through the FFS. The circles are drawn with radii of one and two standard deviations which contain more than 50% and 90% of the beam, respectively.

Figure 3 shows the tolerance of the system to variations in the incident beam momentum spread.

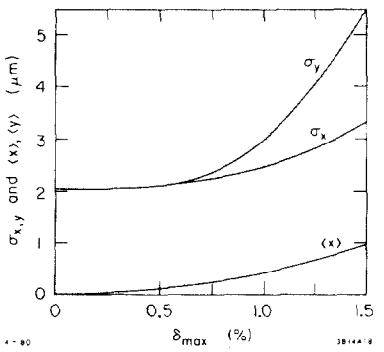

Fig. 3. Predicted beam position and spread at the interaction region as a function of maximum incident momentum δ_{max}. The mean value of vertical position ⟨y⟩ is very small because there are no vertical bending magnets in the system, i.e., $(y|\delta^n)$ and $(y'|\delta^n)$ are negligible so long as there are no significant rotational misalignments.

Ray-Tracing Discussion

The above results were obtained from exact solution of the nonlinear differential equations of motion for the system of Fig. 1 with the fields of Appendix 2. The fields were determined from Taylor expansions through at least the first two leading orders for all multipole fields. A number of checks on all aspects of the calculations were carried out to obtain both accuracy and speed. The results of ray-tracing were analyzed in a number of different ways. For instance, to understand the variation of the mean position of the beam at the IR (⟨x⟩,⟨y⟩ in Fig. 3) and its rms spread, we projected individual rays onto a generalized transfer function which is a power series expansion of the output variables (x_o,x_o', etc.) in terms of the input variables (x_i,x_i', etc.). The complete transfer function through fourth-order was determined in two independent ways. We found the fourth-order chromatic term $(x|y'^2\delta^2) = 3.09$ cm/mr^2/%^{2} dominates ⟨x⟩ whereas the variation of σ_x with incident momentum spread comes from the terms:

$$\begin{aligned}
(x|y'^2\delta) &= -6.8 \quad (\text{cm/mr}^2/\%) \\
(x|yy'\delta) &= 1.6 \quad (\text{cm/cm/mr}/\%) \\
(x|xx'\delta) &= 1.3 \quad (\text{cm/cm/mr}/\%) \\
(x|y'^2\delta^2) &= 3.1 \quad (\text{cm/mr}^2/\%^2)
\end{aligned}$$

The same kind of analysis as for δ_{max} (Fig. 3) can be done for the rest of the input phase space (σ_x,$\sigma_{x'}$, etc.) to show other sensitivities. This is not done except to show one of many plots of the correlation between input and output variables, e.g., x_o and y_i' in Fig. 4. One sees a very fast increase in beam size for $y_i' \geq 7$ μrad, i.e., the system has been well optimized for $\sigma_{y'i} \leq 0.00825$ mr. The rapid increase beyond these values of y_i' is due to some of the previous terms as well as the higher order geometric terms:

$$\begin{aligned}
(x|x'y'^2) &= 297.8 \quad (\text{cm/mr}^3) \\
(x|y'^4) &= 2703. \quad (\text{cm/mr}^4)
\end{aligned}$$

Thus, even for a monochromatic beam we would expect a comparable result in Fig. 3 weighted toward positive values of x_o. Such terms are not easily corrected in optical systems whose highest order multipoles are sextupoles.

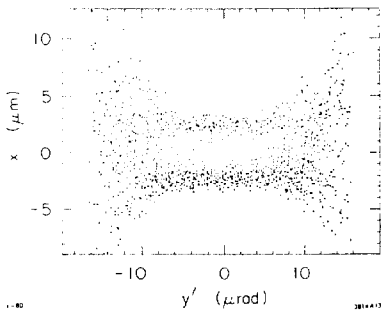

Fig. 4. Results of ray-tracing showing the correlation between the output horizontal position (x_o) at the IR and input vertical angle (y'_i) from the collider lattice.

Appendix 1 - Phase Space Prescription

The ray set which is traced is selected at random by assuming independent normal distributions (ψ) in the transverse coordinates (x,x',y,y') and a square distribution in the energy coordinate (δ) of each particle:

$$\psi(\xi) = \frac{1}{\sqrt{2\pi}\sigma_{\xi i}} e^{-\frac{1}{2}(\xi/\sigma_{\xi i})^2} \quad ; \quad \xi = x, x', y \text{ or } y'$$

$$\psi(\delta) = 2(R - \tfrac{1}{2}) \quad ; \quad 0 \le R \le 1 \quad .$$

The constraints on individual rays are:

$$\left(\frac{x_i}{2\sigma_{xi}}\right)^2 + \left(\frac{x'_i}{2\sigma_{x'i}}\right)^2 \le 1$$

$$\left(\frac{y_i}{2\sigma_{yi}}\right)^2 + \left(\frac{y'_i}{2\sigma_{y'i}}\right)^2 \le 1$$

$$\delta_i = |\delta_{max}|\ \psi(\delta) \quad .$$

For assumed rms standard deviations of:

$$\sigma_{xi} = \sigma_{yi} = 0.03637 \text{ mm}$$
$$\sigma_{x'i} = \sigma_{y'i} = 0.00825 \text{ mr}$$
$$\delta_{max} = \pm 0.5\%$$

the resulting effective rms input spreads using these values and the 2σ-prescription are:

$$\sigma_x = \sigma_y \simeq 0.0300 \text{ mm}$$
$$\sigma_{x'} = \sigma_{y'} \simeq 0.0070 \text{ mr}$$
$$\sigma_\delta \simeq 0.289\%$$

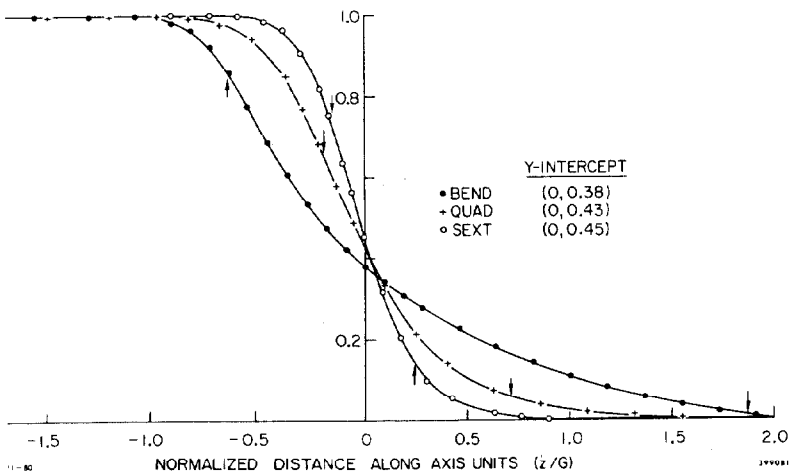

Fig. 5. Dipole, quadrupole and sextupole field distributions normalized to their pure harmonic, central field strengths versus distance along the longitudinal axis normalized to their respective gap openings. The dots (•), pluses (+) and circles (o) are measured field data for the PEP standard bends, quads and sextupoles. The solid curves are fits corresponding to the coefficients of Table I.

Appendix 2 - Field Description

For a right-handed coordinate system with z along the magnet axes (x = 0, y = 0) and the dispersion plane corresponding to the x-z plane (y = 0), we define the normal angular orientation of any multipole about the z-axis so that there is mirror symmetry about the y = 0 plane. This limits the field in the median plane (y = 0) to a single component, $B_y(x,0,z)$, from which the field everywhere B(x,y,z) can be determined to any order based on Maxwell's equations and a general multipole prescription using modified Fermi functions:[4]

$$\text{Dipole:} \quad B_y(0,0,z) = B_0/(1+e^{S_0})$$
$$\text{Quad :} \quad \partial B_y(0,0,z)/\partial x = G_1/(1+e^{S_1})$$
$$\text{Sext :} \quad \partial^2 B_y(0,0,z)/\partial x^2 = 2G_2/(1+e^{S_2}) \quad .$$

S is a polynomial in z normalized to the total gap or bore opening (g) for each multipole. The fifth order polynomial

$$S = C_0 + C_1(z/g) + C_2(z/g)^2 + \ldots + C_5(z/g)^5$$

is sufficient for most cases[4] as shown by the fits to measured data in Fig. 5 for the magnets of the PEP storage ring.[5] None of these magnets were terminated by field clamps so they provide a consistent field description for the SPC. The coefficients are given in Table I.

TABLE I. Field Coefficients

Coefficients	Dipole	Quadrupole	Sextupole
C_0	0.478959	0.296417	0.176659
C_1	1.911289	4.533219	7.153079
C_2	-1.185953	-2.270982	-3.113116
C_3	1.630554	1.068627	3.444311
C_4	-1.082657	-0.036391	-1.976740
C_5	0.318111	0.022261	0.540068

References

1. B. Richter, IEEE Trans. on Nucl. Sci. NS-26, 4261-4265 (1979); B. Richter et al., Proceedings of the XIth International Conference on High Energy Accelerators, CERN, Geneva, Switzerland, July 7-11, 1980. Also SLAC-PUB-2549 (June 1980).
2. SLC Design Report, SLAC-Report-229 (June 1980).
3. K. L. Brown, SLAC-PUB-2257 (February 1979).
4. J. E. Spencer and H. A. Enge, Nucl. Instrum. Methods 49, 181-193 (1967).
5. J. K. Cobb, G. E. Fischer, D. R. Jensen, J. E. Spencer and Zorhab Vassilian, unpublished.